Research Square

Preprints are preliminary reports that have not undergone peer review.
They should not be considered conclusive, used to inform clinical practice,
or referenced by the media as validated information.

Numerical Investigation of Contact Detonation Effects on an Unreinforced Brick Masonry Wall: Charge Configuration, Explosive Type, and Debris Response

Saman Jafari
Bu-Ali Sina University
Farshid Kholoosi
Farshidkholoosi@gmail.com
Bu-Ali Sina University

Research Article

Keywords: Blast loading, Unreinforced masonry, Brick wall, LS-DYNA, SPH, RHT model, Debris velocity

Posted Date: November 18th, 2026

DOI: https://doi.org/10.21203/rs.3.rs-11466849/v1

License: This work is licensed under a Creative Commons Attribution 4.0 International License.
Read Full License

Additional Declarations: No competing interests reported.

Numerical Investigation of Contact Detonation Effects on an Unreinforced Brick Masonry Wall: Charge Configuration, Explosive Type, and Debris Response

Abstract

Masonry walls are widely used in civil engineering and architecture, but their heterogeneous and discontinuous nature makes the numerical simulation of their response to high dynamic loads challenging. In this study, the effects of explosive geometry, charge mass, charge density, and explosive type on the blast-induced damage and debris response of an unreinforced brick wall were investigated using LS-DYNA. The numerical model was first assessed against the 1-kg contact-detonation configuration reported by a reference article. The maximum debris velocity obtained in the present simulation was 67.1 m/s, compared with approximately 70 m/s in the reference numerical model, corresponding to a difference of 4.14%, and 80 m/s in the corresponding experiment. Among the investigated approximately 1-kg contact-detonation configurations, the cubic charge resulted in the highest maximum debris velocity (67.1 m/s), compared with 40.0, 48.2, and 50.3 m/s for the spherical, perpendicular cylindrical, and parallel cylindrical charges, respectively. For the investigated 4-kg configurations, changes in charge volume and density produced configuration-dependent responses: the maximum debris velocity decreased for the spherical and perpendicular cylindrical configurations, while the damage state and kinetic-energy response did not change uniformly across all geometries. Among the investigated explosive types, HMX produced the highest maximum debris velocity of 116.3 m/s, compared with 67.1 m/s for TNT. However, because the explosive materials have different densities, detonation velocities, JWL parameters, and corresponding charge volumes, the individual effects of explosive type and its physical properties cannot be isolated independently from the present comparisons. The results provide a numerical basis for investigating blast-induced damage and debris generation in unreinforced masonry walls subjected to contact detonation.

Keywords: Blast loading; Unreinforced masonry; Brick wall; LS-DYNA; SPH; RHT model; Debris velocity**.**

1. Introduction

The development of reliable numerical approaches for the analysis of masonry structures has received considerable attention because of the heterogeneous nature of masonry, the different mechanical properties of bricks and mortar, and the complex interaction between masonry units and joints. Early experimental and numerical studies established the basis for characterizing masonry constituents and developing appropriate computational models. Bergami [1] investigated the nonlinear behavior of masonry-infilled reinforced-concrete frames and developed numerical models that were assessed through experimental verification. The results demonstrated the importance of an appropriate representation of masonry infill in reproducing the nonlinear structural response and associated failure mechanisms. Grabowski [2] investigated the material properties required for experimental testing and the verification of masonry design models within the ESECMaSE project. The study provided experimentally determined material-property data for masonry components and contributed to the verification of the corresponding design procedures. These studies highlight the importance of accurately characterizing masonry constituents for reliable numerical analysis. Lourenço [3] investigated computational strategies for masonry structures and discussed different levels of numerical

representation, including detailed micro-modeling, simplified micro-modeling, and macro-modeling. The study emphasized that the appropriate modeling strategy depends on the required level of detail, computational cost, and structural behavior to be reproduced. Barraza [4] developed a numerical model for the nonlinear analysis of masonry walls, with particular attention to nonlinear material behavior and masonry failure mechanisms. The results further demonstrated the importance of an appropriate numerical representation for reproducing cracking and nonlinear response. Giambanco and Di Gati [5] proposed a cohesive interface model for the structural mechanics of block masonry to represent the mechanical behavior of masonry interfaces. Their approach accounted for the transmission of stresses across interfaces and the progressive separation and failure of masonry components, highlighting the importance of interface behavior in reproducing cracking and discontinuous failure. Dynamic loading of masonry has also been investigated using numerical approaches that account for the interaction between masonry units and interfaces. Burnett et al. [6] developed a finite-element approach for analyzing unreinforced brickwork and blockwork walls subjected to low-velocity out-of-plane impacts. The masonry units were modeled using linear-elastic solid elements, while a specialized interface formulation was employed to represent the masonry joints. The interface model incorporated a Mohr–Coulomb failure criterion, cohesive cracking, and dilatancy. The numerical simulations provided reasonable predictions of the observed wall response and demonstrated the importance of interface properties and failure mechanisms in impact analysis. Lopez et al. [7] proposed a homogeneous constitutive model for masonry based on homogenized anisotropic elastoplasticity. Their approach represented masonry as an equivalent continuum while retaining its principal directional characteristics, providing a computationally efficient alternative to detailed micro-modeling. Anthoine [8] investigated the derivation of the in-plane elastic characteristics of masonry using homogenization theory. The study derived effective masonry properties from the characteristics and arrangement of bricks and mortar and examined the influence of masonry geometry and bond pattern on the resulting elastic response. Chen et al. [9] developed a macroelement for the nonlinear analysis of in-plane unreinforced masonry piers. The proposed formulation incorporated axial, shear, and rotational components to represent the principal nonlinear mechanisms observed in masonry, including sliding, diagonal cracking, rocking, and crushing. The model provided an efficient approach for reproducing the nonlinear response of masonry components while reducing the computational cost associated with detailed modeling. Bogosian and Gerber [10] investigated fragment penetration through hollow concrete masonry units using the AUTODYN code and the smoothed particle hydrodynamics (SPH) method. The effects of fragment size on the resulting hole dimensions, surrounding damage, and residual fragment velocity were examined. The numerical predictions were compared with established analytical and empirical relationships and were shown to reproduce the main trends associated with fragment penetration and masonry damage. This study also demonstrated the importance of appropriate numerical treatment of highly fragmented masonry and the subsequent motion of fragments. For explosion-related problems, an appropriate representation of the explosive loading is an additional requirement for reliable numerical analysis. Randers-Pehrson and Bannister [11] developed an airblast loading model for DYNA2D and DYNA3D based on the CONWEP formulation. The model provides a practical approach for applying airblast loads to structures without explicitly modeling the surrounding air domain. Wang [12] investigated the numerical simulation of landmine explosions using LS-DYNA 3D and presented benchmark simulations for explosions in soil and air. The study demonstrated the applicability of LS-DYNA3D for simulating explosion-related loading and structural response. Williams et al. [13] investigated the validation of a loading model for simulating blast-mine effects on armored vehicles. Their study

demonstrated the importance of an appropriately calibrated blast-loading formulation for reproducing the loading generated by explosive events and predicting the resulting structural response. Kingery and Bulmash [14] established a widely used set of empirical airblast parameters for TNT spherical air bursts and hemispherical surface bursts. Their work has provided the basis for several engineering methods used to estimate conventional airblast parameters. However, such empirical airblast relationships are primarily intended for free-field airblast conditions and are not directly representative of the highly localized interaction between an explosive charge and a masonry wall under contact detonation. Several experimental studies have investigated methods for improving the mechanical resistance of unreinforced masonry walls through strengthening techniques. Lin et al. [15] experimentally investigated the out-of-plane behavior of unreinforced masonry walls strengthened using engineered cementitious composite (ECC) shotcrete. Their results demonstrated a substantial improvement in the out-of-plane resistance of the strengthened walls, confirming the effectiveness of ECC shotcrete as a strengthening technique. Lin et al. [16] investigated the in-plane strengthening of clay-brick unreinforced masonry wallettes using ECC shotcrete. The experimental results showed a significant increase in strength compared with unstrengthened specimens, while the increase in performance became less pronounced with increasing ECC thickness. These studies demonstrated the potential of ECC-based strengthening for improving the structural resistance of unreinforced masonry walls under mechanical loading. Maalej et al. [17] investigated the use of engineered cementitious composites for strengthening unreinforced masonry walls under quasi-static and dynamic loading, including low-velocity impact. Their experimental results showed that ECC strengthening can improve the load-carrying capacity and ductility of masonry walls and enhance their resistance to repeated low-velocity impacts. Dizhur et al. [18] investigated the out-of-plane strengthening of unreinforced masonry walls using near-surface-mounted fiber-reinforced polymer strips. Their experimental results demonstrated that the proposed strengthening technique can significantly improve the out-of-plane resistance of unreinforced masonry walls. These studies primarily addressed structural and seismic strengthening rather than the response of unreinforced masonry walls to direct explosive loading. Khooshechi and Tanzadeh [19] experimentally investigated the mechanical performance of shotcrete incorporating nanomaterials and fiber reinforcement. Their results showed that the incorporation of nanomaterials and fibers can modify the mechanical and cracking characteristics of shotcrete. Although the study did not directly investigate blast-loaded masonry walls, it provides relevant information concerning the mechanical characteristics of cementitious strengthening materials. Mardani et al. [20] presented a design example for the seismic retrofit of a two-story unreinforced masonry building using shotcrete. The study evaluated the seismic vulnerability of the building and proposed shotcrete-based retrofit measures to improve its structural performance. Thus, this study also focused on seismic strengthening rather than explosive loading. Among the studies directly related to explosive loading of masonry, Michaloudis and Gebbeken [21] investigated the numerical modeling of unreinforced masonry walls subjected to both far-field and contact detonations. Their study addressed the selection and adaptation of a material formulation capable of representing the behavior of bricks under high strain rates and investigated the formation of local damage and debris under explosive loading. In particular, the authors showed that small portions of the wall near the explosive can separate from the main wall and travel at high velocities, creating an additional hazard beyond the directly damaged region. The numerical results were compared with experimental observations and showed good agreement. The study further indicated that interface modeling is particularly important for far-field detonation, whereas the formulation of the equation of state becomes especially important for contact detonation. Despite the progress

achieved in the numerical modeling of masonry under dynamic and explosive loading, there remains a need for a systematic investigation of the influence of the characteristics of the explosive charge on the response of unreinforced brick masonry under contact detonation. However, comparatively limited attention has been given to systematically examining the combined influence of explosive geometry, charge mass, charge density, and explosive type within a consistent numerical framework for the same masonry configuration. Therefore, in the present study, LS-DYNA is employed to investigate the response of an unreinforced brick wall subjected to contact detonation. First, the numerical approach is assessed against the 1-kg contact-detonation configuration reported by Michaloudis and Gebbeken [21]. Subsequently, a parametric investigation is conducted to examine the effects of explosive geometry, charge mass, charge density, and explosive type on wall damage and debris response. The results provide a systematic assessment of how the characteristics of the explosive charge influence the severity of damage and the subsequent motion of masonry debris under contact detonation.Despite the progress achieved in the numerical modeling of masonry under dynamic and explosive loading, comparatively limited attention has been given to the combined influence of explosive geometry, charge mass, charge density, and explosive type on the response of unreinforced brick walls subjected to contact detonation. In particular, the relationship between charge configuration and debris response, including debris velocity and kinetic energy, requires further investigation. Therefore, the present study uses LS-DYNA to investigate the effects of these parameters on wall damage and debris response. The numerical approach is first assessed against the 1-kg contact-detonation configuration reported by Michaloudis and Gebbeken [21], followed by a parametric investigation using different explosive configurations.

2. Numerical Model and Validation Configuration

Michaloudis and Gebbeken [21] investigated the response of masonry walls subjected to far-field and contact detonations. Their study included far-field explosions with charge masses of 810 and 1150 kg at a distance of 37 m, as well as contact detonations with charge masses of 0.25 and 1 kg. In the present study, the 1-kg contact-detonation case was selected to assess the numerical model.

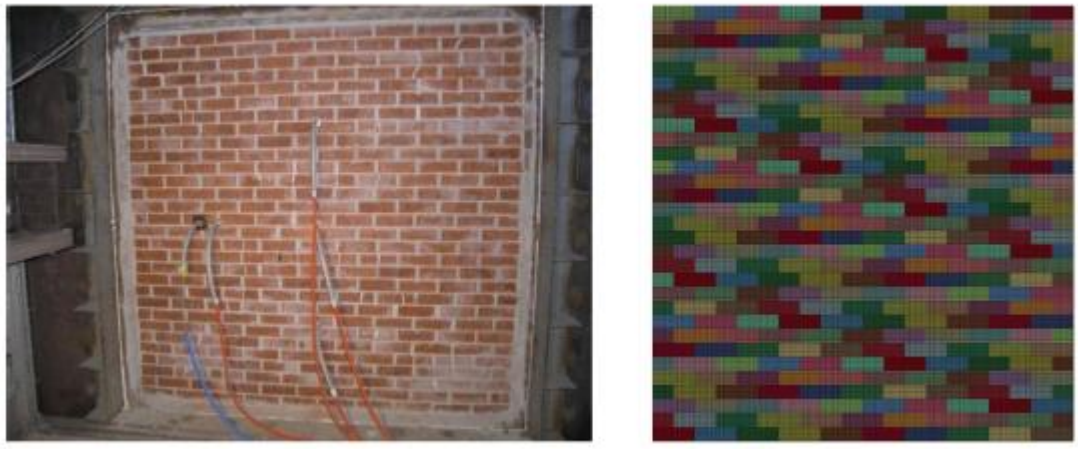
2.1. Material Properties

In Ref. [21], TNT was used to blast a brick wall. The properties of TNT are presented in the table below.

Table 1. Properties of TNT used in the validation case [21].

Pressure	Detonation velocity	Density
(Pa)	(m/s)	(kg/m^3)
2.1×10^{10}	6930	1500

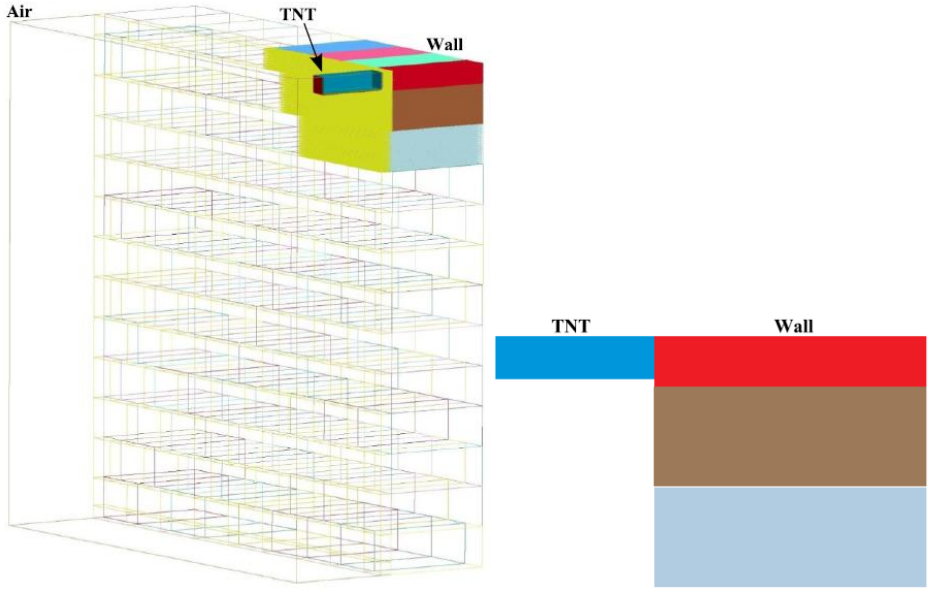
The overall dimensions of the wall under study are 2 × 2 meters, and the dimensions of each brick are 24 × 8 × 12 centimeters. Fig. 1 shows the wall under study in the experimental and simulation methods. In Abaqus software, the bricks were modeled individually in meters and then entered into LS-DYNA software to analyze the explosion problem.



a b

Fig. 1. Experimental and numerical models of the masonry wall: (a) experiment and (b) numerical model.

As mentioned earlier, in Ref. [21], four cases were studied to investigate the parameters affecting the destruction of the wall. In this study, case 4 from this reference was used for validation. In this case, the explosive was attached to the wall. The mass of the explosive was also considered to be 1 kg. Fig. 2 shows the explosive attached to the wall. In this Fig, a quarter of the wall is shown.



Perspective view detailed side view at the proximity of the explosive material

Fig. 2. Wall geometry and explosive [21].

In the simulation of Ref. [21], the RHT material model in LS-DYNA was used to define the material properties of the bricks. Table 2 presents the material properties of the bricks. In the simulation, the properties listed in Table 2 were defined individually for each brick, meaning that each brick was modeled as a separate section.

Table 2. Brick material properties used in the RHT model [21].

Parameter	Amount	Unit	Source
Shear Modulus, G	1.023×10^{9}	(Pa)	Experiments
Compressive strength, fc	13.5×10^{6}	(Pa)	Experiments
Tensile/compressive strength, ft/ fc	0.0813	-	Experiments
Shear/compressive strength, fs/fc	0.1078	-	Experiments
Failure surface parameter, A	1.6	-	Adaptation
Failure surface parameter, N	0.95	-	Adaptation
Brittle/ductile behavior factor, Q_0	0.76	-	Adaptation
Brittle/ductile behavior factor, B	1×10^{-5}	-	Adaptation
Yield surface parameter, gt*	0.2222	-	Experiments
Yield surface parameter, gc^*	0.4434	-	Experiments
Residual surface parameter, A_F	1.6	-	Adaptation
Residual surface parameter, N_F	0.95	-	Adaptation
Compressive strain-rate exponent, βc	0.066083	-	Adaptation
Tensile strain-rate exponent, βt	0.059684	-	Adaptation

All RHT material parameters required for the numerical implementation, including the density and equation-of-state parameters, were assigned according to the calibrated brick material formulation reported in Ref. [21]. The parameters listed in Table 2 correspond to the material quantities explicitly reported and used to characterize the brick response in the present model.

2.2. Boundary Conditions and Contact Definitions

In Ref. [21], the wall under study was considered to be completely fixed. The interaction between the explosive and the wall was defined using an automatic node-to-surface contact formulation. The interaction between adjacent bricks was modeled using the Contact_Automatic_One_Way_Surface_To_Surface_Tiebreak formulation. This interface formulation was used to represent the mechanical behavior and failure of the mortar joints without explicitly modeling the mortar as a separate solid domain. The normal and shear failure parameters adopted for the contact interfaces are listed in Table 3. To assess the reliability of the numerical model, the 1-kg contact-detonation case reported by Michaloudis and Gebbeken [21] was reproduced using the same general wall configuration and explosive mass. In the reference study, both far-field and contact-detonation cases were investigated. The present validation focuses on the contact-detonation case in which a 1-kg TNT charge was attached directly to the wall. The wall dimensions, individual brick dimensions, TNT properties, and the RHT material model used for the brick material were defined according to the information reported in Ref. [21]. The corresponding model configuration is shown in Figs. 1 and 2.

Table 3. Interface failure parameters used between adjacent bricks [21].

Parameter	Unit	Amount
Ultimate stress in normal direction	[Pa]	110×10^{3}
Ultimate stress in shear direction	[Pa]	440×10^{3}
Energy release rate in normal direction	[Pa.m]	61.6
Energy release rate in shear direction	[Pa.m]	246.4

2.3. Numerical Discretization and Solution Settings

The masonry wall was discretized using three-dimensional eight-node hexahedral solid elements with a one-point integration formulation (ELFORM = 1). The mesh dimensions were adopted from the numerical modeling approach of Michaloudis and Gebbeken [21]. Accordingly, elements measuring 2.5 × 2.5 × 2.5 mm were employed in the region near the contact detonation, while elements with a side length of 5 mm were used in the remaining regions of the wall. This discretization was selected to provide a refined representation of the localized damage and debris formation near the explosive charge. The adequacy of the adopted numerical model was subsequently assessed through comparison with the reference results in the validation section.

Unlike the Eulerian–Lagrangian approach used in Ref. [21], the explosive charges in the present study were modeled using the smoothed particle hydrodynamics (SPH) method. The SPH formulation was defined using the SECTION_SPH and CONTROL_SPH keywords. The smoothing-length parameters CSLH, HMIN, and HMAX were set to 1.2, 0.2, and 2.0, respectively. The SPH control parameters included NCBS = 2, IDIM = 3, and FORM = 5.

The interaction between the relevant model components was defined using the CONTACT_AUTOMATIC_NODES_TO_SURFACE formulation. The contact definition included the slave and master entities identified by IDs 100005 and 26, respectively, with SSTYP = 3 and MSTYP = 2. The global contact settings were specified through CONTROL_CONTACT, including the penalty stiffness scale factor SLSFAC = 0.1. The explosive initiation was defined using INITIAL_DETONATION at the prescribed initiation point.

Boundary conditions were applied using BOUNDARY_SPC_SET to constrain the supported regions of the masonry wall. Consistent with the reference modeling approach [21], the translational degrees of freedom along the supported boundaries were restrained. This numerical configuration was used for the subsequent parametric investigation of explosive geometry, charge mass, charge density, and explosive type on wall damage and debris response.

3. Validation

The numerical model was validated against the 1-kg TNT contact-detonation case reported by Michaloudis and Gebbeken [21]. In the reference study, a TNT charge with a mass of 1 kg was attached directly to the masonry wall. The same contact-detonation configuration was reproduced in the present study using the wall geometry, brick dimensions, material properties, boundary conditions, and interface properties reported in Ref. [21]. Fig. 3 presents the numerical simulation of the wall destruction reported in Ref. [21] for the 1-kg contact-detonation case.

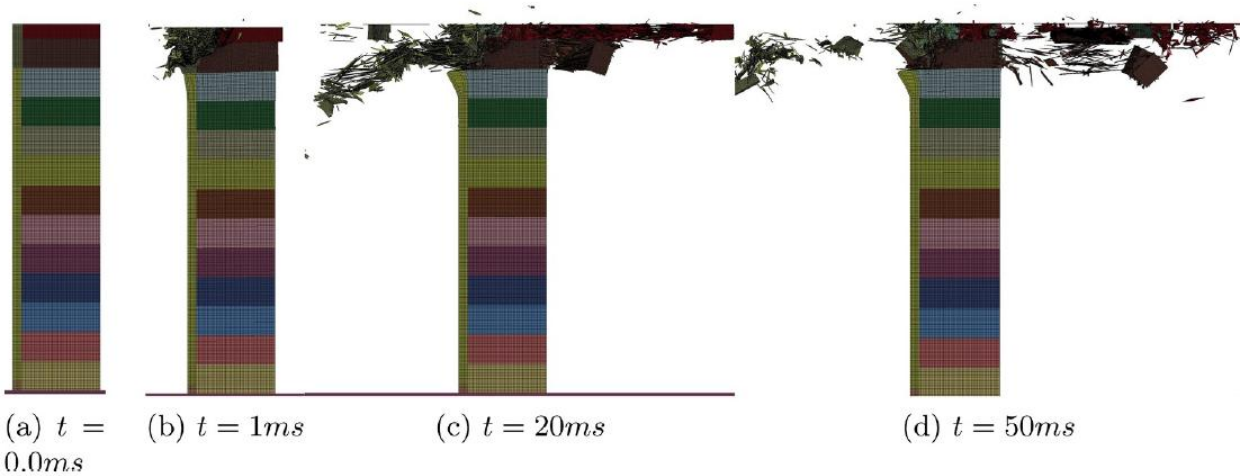


Fig. 3. Numerical simulation of masonry wall destruction under 1-kg TNT contact detonation reported in Ref. [21].

Fig. 4 shows the numerical model developed in the present study. The TNT charge was attached directly to the wall, and its mass was set to 1 kg. The overall wall dimensions and individual brick dimensions were defined according to Ref. [21]. The material properties of the bricks were described using the RHT material model, and the interface properties between adjacent bricks were defined according to the reference study.

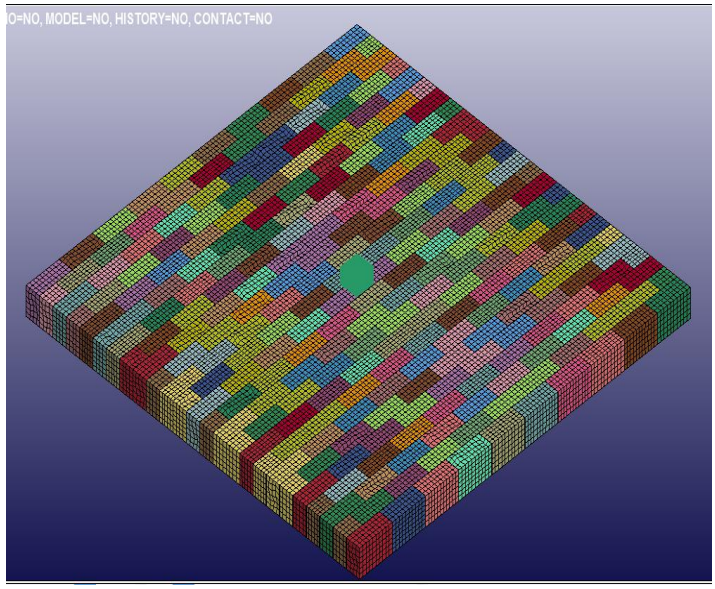


Fig. 4. Numerical model of the masonry wall subjected to 1-kg TNT contact detonation in the present study.

In Ref. [21], the TNT charge and surrounding air were modeled using an Eulerian formulation, while the masonry wall was represented using a Lagrangian formulation. In the present study, the TNT charge was modeled using the SPH formulation. This formulation was adopted to

represent the large deformation and rapid expansion of the explosive material while avoiding excessive distortion of conventional solid elements. The remaining modeling parameters, including the wall geometry, brick material model, boundary conditions, and interface properties, were kept consistent with the reference configuration as far as the available information allowed. Fig. 5 presents the evolution of the masonry wall damage following detonation. Immediately after detonation, severe damage develops in the region surrounding the explosive charge. With increasing time, the damaged region expands, and individual bricks become detached from the main wall and move away from the wall surface. The predicted damage evolution and debris formation are qualitatively consistent with the characteristic response reported in Ref. [21].

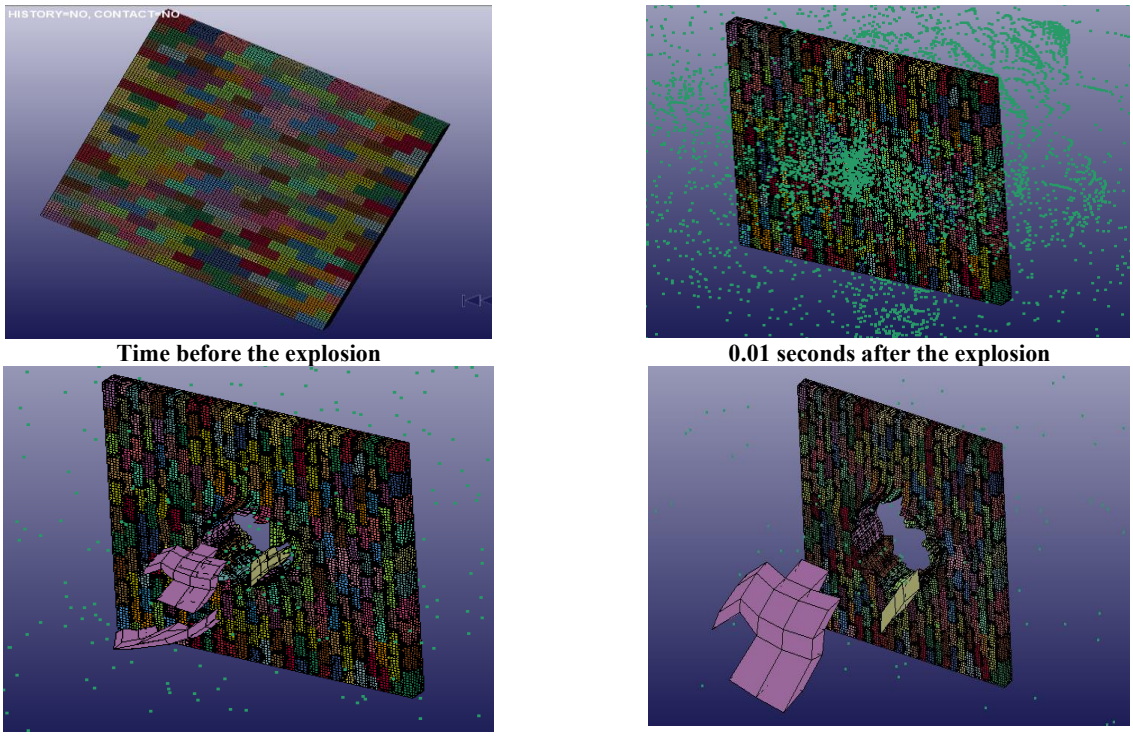


Fig 5. Evolution of masonry wall damage following the contact detonation of 1-kg TNT at t = 0, 10, 30, and 50 ms.

A quantitative comparison was performed using the maximum velocity of the detached masonry debris. Fig. 6 presents the velocity histories of the individual bricks detached from the wall during the detonation process. The maximum debris velocity obtained in the present simulation was 67.1 m/s.

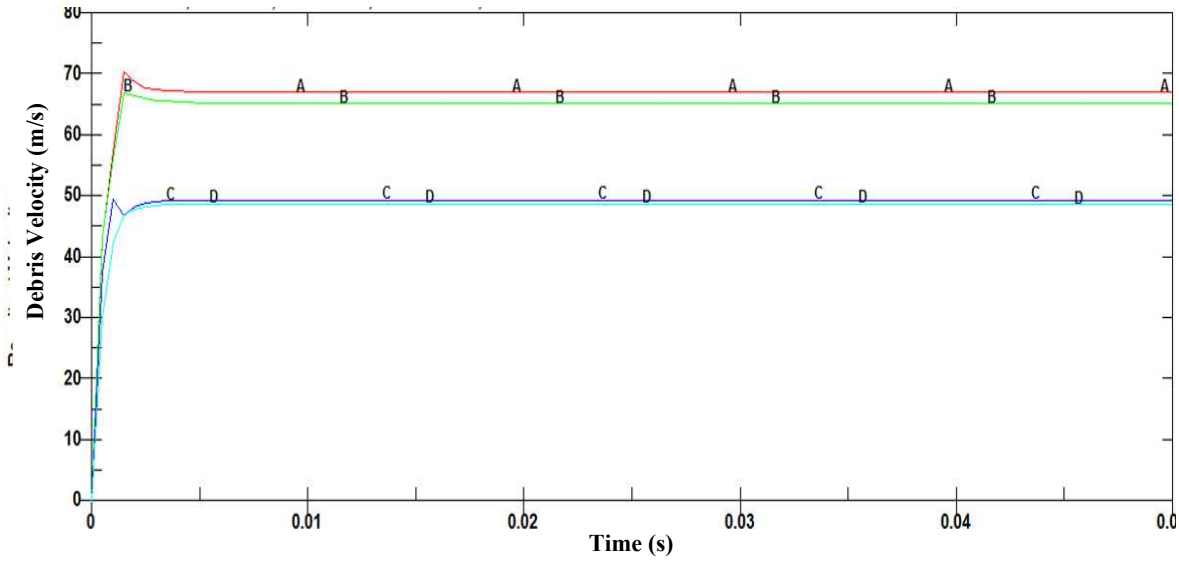


Fig. 6. Velocity histories of individual bricks detached from the masonry wall during the contact detonation of 1-kg TNT.

As shown in Table 4, the maximum debris velocity obtained in the present study was 67.1 m/s, compared with approximately 70 m/s in the numerical model of Ref. [21] and approximately 80 m/s in the corresponding experiment. The relative difference between the present numerical result and the reference numerical result is 4.14%, whereas the difference from the experimental result is approximately 16.2%. The close agreement between the present numerical result and the numerical result of Ref. [21] indicates that the present model provides a consistent prediction of the debris velocity for the investigated contact-detonation configuration. The larger difference from the experimental result may be attributed to the inherent differences between the numerical and experimental representations of masonry behavior, brick–mortar interaction, explosive–wall interaction, and other numerical idealizations. The validation should therefore be considered a partial assessment of the numerical model for the investigated 1-kg contact-detonation configuration rather than a comprehensive validation over a wide range of explosive loading conditions. The agreement in maximum debris velocity, together with the qualitative consistency of the predicted damage evolution, provides a reasonable basis for conducting the subsequent numerical parametric investigation.

Table 4. Quantitative comparison of the maximum debris velocity for the 1-kg contact-detonation case.

Case	Maximum debris velocity (m/s)	Absolute difference (m/s)	Relative difference (%)
Present study	67.1	-	
Ref. [21], numerical	70	2.9	4.14
Ref. [21], experiment	80	12.9	16.2

4. Studied Geometries

Figs. 7–10 show the different explosive geometries considered in the contact-detonation simulations. For the cubic geometry attached to the wall, the effects of four different types of explosives were investigated, and the properties of these materials are presented in Table 5 [22].

5. Geometrical Characteristics, Mass, Density, and Properties of Explosives

Table 5 presents the material properties and JWL equation-of-state parameters of the explosives considered in this study. In the JWL formulation, A, B, R1, R2 and ω are explosive-specific parameters, V is the relative specific volume, and E_0 is the initial specific internal energy of the explosive. The TNT parameters were adopted from Ref. [21], while the parameters of HMX, HNS, and Tetryl were obtained from Ref. [22].

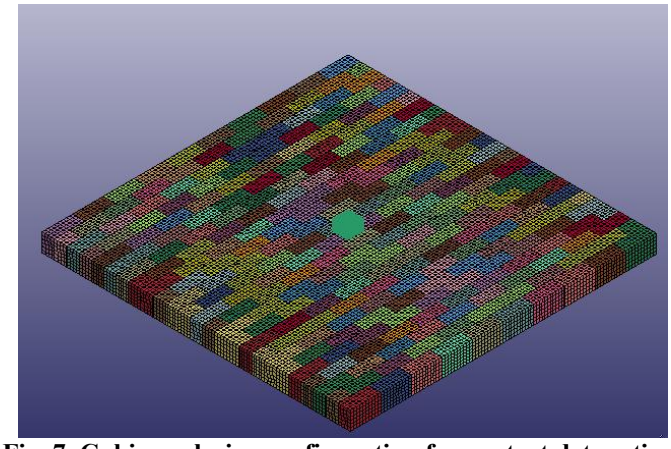


Fig. 7. Cubic explosive configuration for contact detonation.

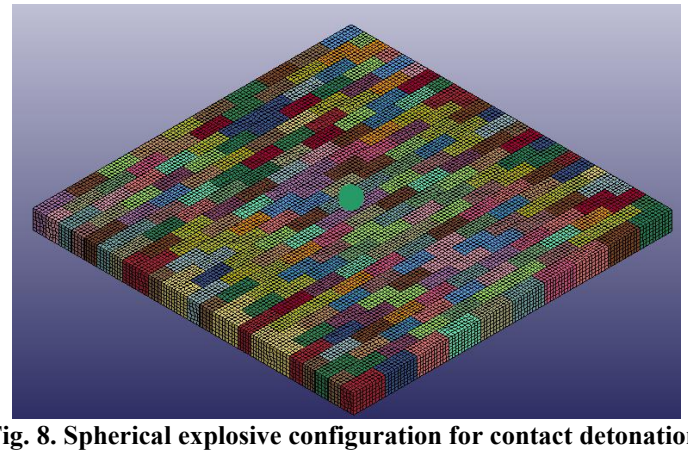


Fig. 8. Spherical explosive configuration for contact detonation.

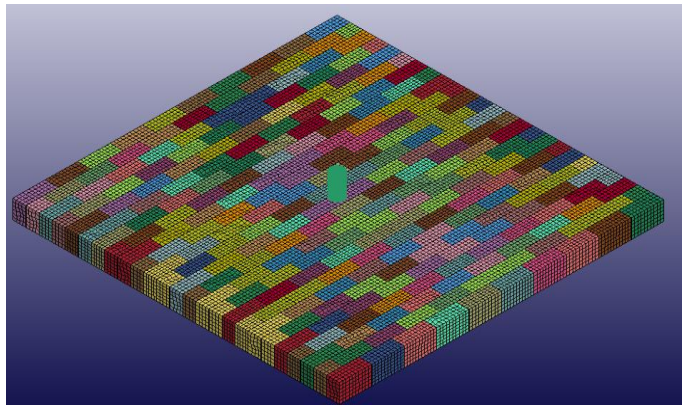


Fig. 9. Cylindrical explosive configuration perpendicular to the wall surface for contact detonation.

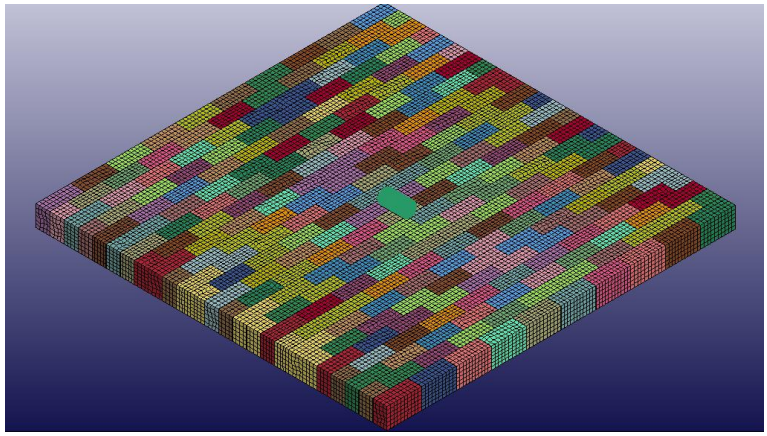


Fig. 10. Cylindrical explosive configuration parallel to the wall surface for contact detonation.

Table 5. Material properties and JWL parameters of the investigated explosives.

Type	Density (kg/m^3)	Detonation velocity (m/s)	Pressure Chapman–Jouguet (Pa)	A (Pa)	B (Pa)	R1	R2	ω	E0
TNT	1500	6930	2.1×10^{10}	3.71×10^{11}	3.29×10^{9}	4.15	0.95	0.3	4×10^{9}
HMX	1890	9100	4.2×10^{10}	7.78×10^{11}	7.04×10^{9}	4.2	1	0.2	10×10^{9}
HNS	1650	7030	2.15×10^{10}	4.63×10^{10}	8.87×10^{9}	4.55	1.35	0.35	7×10^{9}
TETRYL	1730	7910	2.85×10^{10}	5.6×10^{10}	10.6×10^{9}	4.4	1.2	0.28	8.2×10^{9}

Tables 6–9 summarize the geometry, density, mass, and dimensions of the explosive charges investigated in the contact-detonation simulations. The density is given in kg/m^3, the mass in kg, and the geometric dimensions in m. The dimensions of each explosive geometry were determined from the prescribed explosive mass and density, and the resulting dimensions were used in the numerical models. For the SPH2, CYV2, and CYH2 configurations, a hypothetical density of 6067 kg/m^3 was assigned to increase the charge mass while maintaining approximately the same charge volume. This density does not represent the actual density of TNT and was used only for the numerical parametric comparison. Therefore, the corresponding results should be interpreted as hypothetical numerical cases rather than physically realizable TNT charge configurations.

Table 6. Specifications of the cubic explosive charges.

Geometry	Abbreviation symbol	Density (kg/m^3)	Mass (kg)
Cube 1	Cu1	1500	0.98
Cube 2	HMX	1890	1.18
Cube 3	HNS	1650	1.03
Cube 4	TETRYL	1730	1.08

Table 7. Specifications of the spherical explosive charges.

Geometry	Abbreviation symbol	Density (kg/m^3)	Mass (kg)	(m) Radius
Sphere 1	SPH 1	1500	1	0.054
Sphere 2	SPH 2	6067	4	0.054
Sphere 3	SPH 3	1500	4	0.086

Table 8 Specifications of the cylindrical explosive charges oriented perpendicular to the wall surface.

Geometry	Abbreviation symbol	Density (kg/m^3)	Mass (kg)	Radius (m)	Cylinder length (m)
Cylinder perpendicular to wall surface 1	CYV 1	1500	1	0.0375	0.15
Cylinder perpendicular to wall surface 2	CYV 2	6067	4	0.0375	0.15
Cylinder perpendicular to wall surface 3	CYV 3	1500	4	0.0752	0.15

Table 9. Specifications of the cylindrical explosive charges oriented parallel to the wall surface.

Geometry	Abbreviation symbol	Density (kg/m^3)	Mass (kg)	Radius (m)	Cylinder length (m)
Cylinder parallel to wall surface 1	CYH 1	1500	1	0.0375	0.15
Cylinder parallel to wall surface 2	CYH 2	6067	4	0.0375	0.15
Cylinder parallel to wall surface 3	CYH 3	1500	4	0.0752	0.15

6. Results

For the purposes of this study, wall failure refers to extensive damage accompanied by the separation of a substantial portion of the masonry wall. Local damage refers to cracking or limited brick separation without extensive wall failure. Cracking without brick detachment refers to cases in which cracking develops but no bricks become completely detached from the wall. Figs. 11–14 show the damage patterns of the masonry wall for the investigated explosive geometries. The model specifications are identified by the corresponding abbreviations listed in Tables 6–9. For the cubic configuration, the charge attached to the wall produces damage concentrated around the central region of the wall.

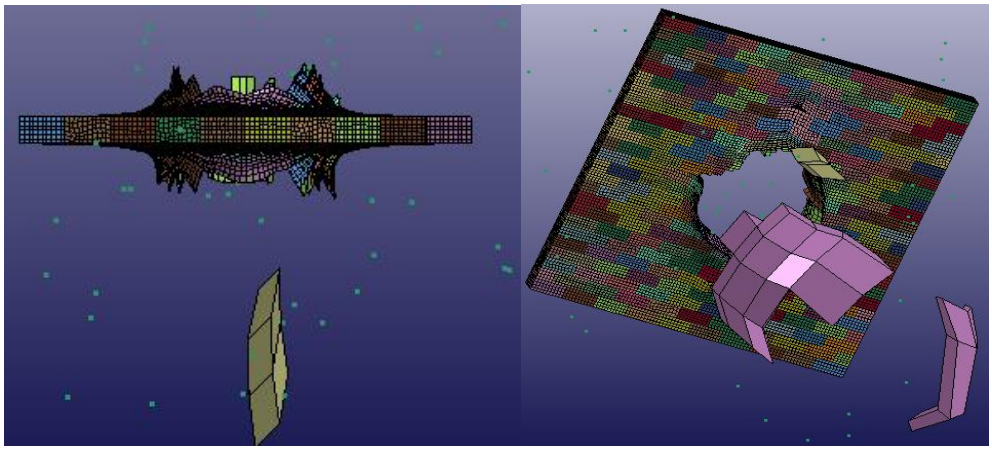
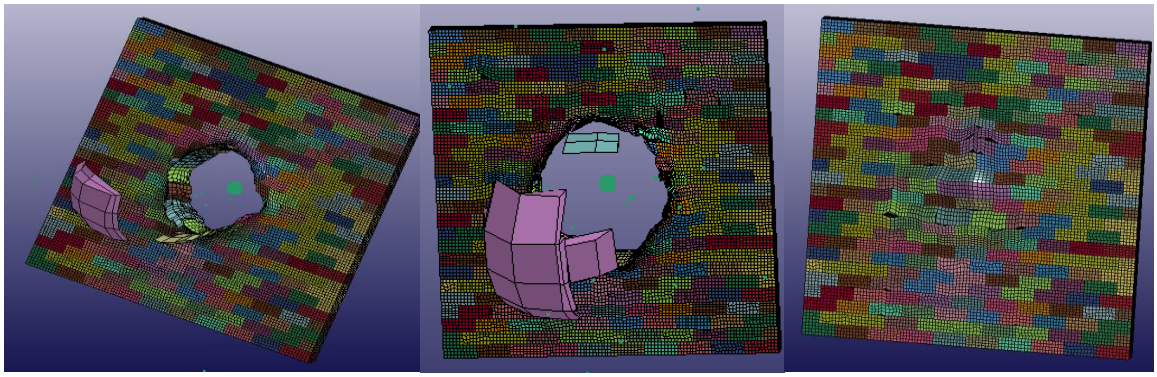


Fig. 11. Damage pattern of the masonry wall subjected to contact detonation of the cubic TNT charge (Cu1).

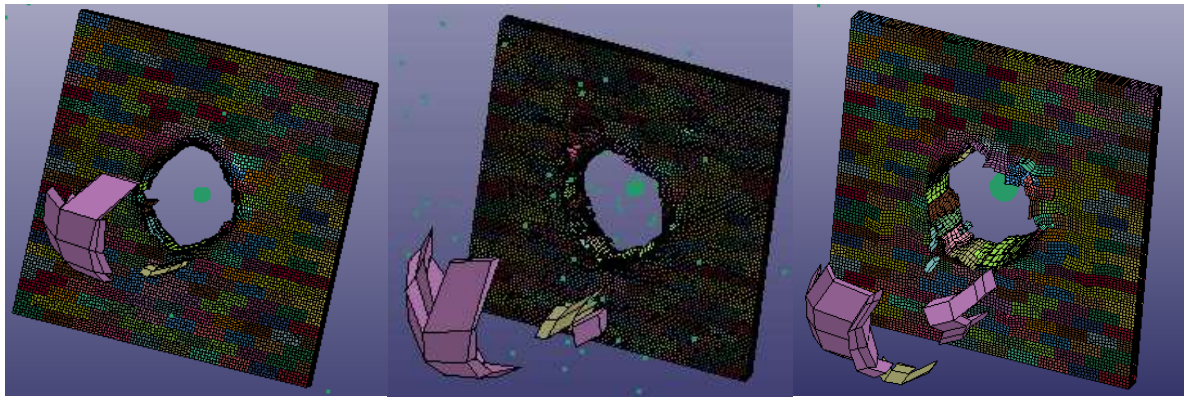
According to Fig. 12, the spherical configurations show different damage responses depending on the charge mass, density, and volume. For SPH1 and SPH2, increasing the explosive mass from 1 to 4 kg while maintaining the same charge radius increased the maximum debris velocity from 40.0 to 43.1 m/s. Because the charge radius was unchanged, the corresponding charge volume remained approximately constant, while the explosive density increased from 1500 to 6067 kg/m³. Despite the increase in charge mass and density, the observed damage state was less severe for SPH2, for which cracking occurred without complete brick detachment, whereas complete wall failure was observed for SPH1. For SPH2 and SPH3, the explosive mass remained constant at 4 kg, while the density decreased from 6067 to 1500 kg/m³ and the charge volume increased. Under these conditions, no complete brick detachment was observed for SPH3. Therefore, the difference between SPH2 and SPH3 represents the combined effect of charge density and volume at approximately constant explosive mass. These results indicate that the structural response cannot be predicted from charge mass alone and depends on the combined characteristics of the explosive configuration. The quantitative results further indicate that the increase in charge mass did not produce a proportional increase in the debris response for the spherical configuration. Increasing the charge mass from 1 kg (SPH1) to 4 kg (SPH2) increased the maximum debris velocity from 40.0 to 43.1 m/s, corresponding to an increase of approximately 7.8%, while the maximum debris kinetic energy increased from 1180 to 1450 J, or approximately 22.9%. Despite these increases in the kinematic response, the observed damage state changed from complete wall failure for SPH1 to cracking without complete brick detachment for SPH2. This non-monotonic response indicates that maximum debris velocity and total debris kinetic energy do not necessarily provide a direct measure of the extent of wall failure. The result also highlights the importance of charge density and volume, which changed simultaneously with the charge mass in the investigated configurations. The numbers 1 to 3 represent the different spherical explosive configurations listed in Table 7.



a b c

Fig. 12. Damage patterns of the masonry wall subjected to contact detonation of spherical explosive charges: (a) SPH 1, (b) SPH 2, (c) SPH 3.

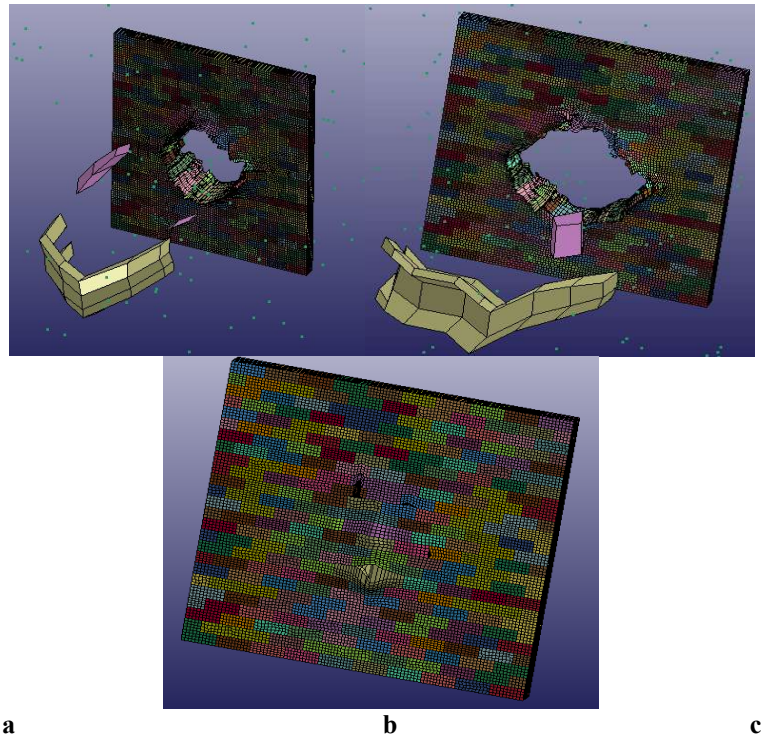
According to Fig. 13, the damage pattern of the cylindrical explosive charges oriented perpendicular to the wall surface is similar to that observed for the spherical configuration, with the most severe damage occurring when the charge is attached to the wall. For CYV1 and CYV2, increasing the charge mass from 1 to 4 kg while maintaining the same cylinder radius and length resulted in an increase in maximum debris velocity from 48.2 to 55.4 m/s. Because the geometric dimensions were unchanged, the charge volume remained approximately constant, while the explosive density increased from 1500 to 6067 kg/m³. The CYV2 configuration consequently produced a larger observed damage region and a higher debris velocity than CYV1. For CYV2 and CYV3, the explosive mass remained constant at 4 kg, while the charge radius increased and the explosive density decreased, resulting in a larger charge volume. Under these conditions, the maximum debris velocity decreased from 55.4 to 43.5 m/s, although complete wall failure was still observed. Therefore, the difference between CYV2 and CYV3 reflects the combined influence of charge volume and density at approximately constant explosive mass. The results indicate that changes in charge geometry and density can modify the debris response even when the total explosive mass remains unchanged. A comparison of the quantitative response also shows that the effect of the charge configuration cannot be characterized by debris velocity alone. For CYV1, CYV2, and CYV3, the maximum debris velocities were 48.2, 55.4, and 43.5 m/s, respectively, whereas the corresponding maximum debris kinetic energies were 1150, 1750, and 2070 J. In particular, CYV3 produced a lower maximum debris velocity than CYV2, while its maximum debris kinetic energy was higher. This difference suggests that the two configurations generated different distributions of mass and velocity among the detached debris. Therefore, the maximum velocity of an individual debris fragment and the total kinetic energy of the tracked debris should be considered complementary measures of the structural response rather than interchangeable indicators. The numbers 1 to 3 represent the different cylindrical explosive configurations listed in Table 8.



a b c

Fig 13. Damage patterns of the masonry wall subjected to contact detonation of cylindrical explosive charges perpendicular to the wall surface: (a) CYV 1, (b) CYV 2, and (c) CYV 3.

Fig. 14 shows the damage patterns produced by cylindrical charges oriented parallel to the wall surface. For CYH1 and CYH2, increasing the explosive mass from 1 to 4 kg while maintaining the same cylinder radius and length increased the maximum debris velocity from 50.3 to 53.7 m/s. Since the geometric dimensions remained unchanged, the charge volume was approximately constant, while the explosive density increased from 1500 to 6067 kg/m³. However, the observed damage state changed from complete wall failure for CYH1 to cracking without complete brick detachment for CYH2. For CYH2 and CYH3, the explosive mass remained constant at 4 kg, while the density decreased from 6067 to 1500 kg/m³ and the charge volume increased. Under these conditions, no complete brick detachment was observed for CYH3. Thus, the difference between CYH2 and CYH3 represents the combined effect of charge density and volume at approximately constant explosive mass. These results further demonstrate that the structural response depends on the complete charge configuration rather than on explosive mass alone. The quantitative results for the parallel cylindrical charges show a similar non-monotonic relationship between debris velocity, kinetic energy, and damage state. Increasing the charge mass from 1 kg (CYH1) to 4 kg (CYH2) increased the maximum debris velocity only from 50.3 to 53.7 m/s, corresponding to an increase of approximately 6.8%. In contrast, the maximum debris kinetic energy decreased from 4290 to 3200 J. At the same time, the observed damage changed from complete wall failure to cracking without complete brick detachment. This indicates that increasing charge mass did not result in a proportional increase in the structural response for this configuration. The different trends in debris velocity and kinetic energy further demonstrate that the manner in which explosive energy is transferred to the masonry and subsequently distributed among the debris depends on the charge configuration.



a b c

Fig. 14. Damage patterns of the masonry wall subjected to contact detonation of cylindrical explosive charges parallel to the wall surface: (a) CYH 1, (b) CYH 2, and (c) CYH 3.

Taken together, the investigated approximately 1-kg configurations demonstrate that explosive geometry and orientation influence the debris response in different ways. The cubic configuration produced the highest maximum debris velocity (67.1 m/s), followed by the parallel cylindrical (50.3 m/s), perpendicular cylindrical (48.2 m/s), and spherical (40.0 m/s) configurations. However, the corresponding maximum debris kinetic energies were not ordered in the same manner. In particular, the parallel cylindrical configuration produced the highest maximum kinetic energy (4290 J), despite having a substantially lower maximum debris velocity than the cubic configuration (2040 J). This difference demonstrates that the geometry of the charge affects not only the maximum velocity reached by individual debris fragments but also the distribution of kinetic energy within the detached material. Consequently, the severity of the debris response is better characterized by considering velocity, kinetic energy, and observed damage state together. Table 10 shows the maximum velocity of the bricks thrown from the wall. Figs. 15 and 16 also show the velocity histories of representative detached bricks and the maximum kinetic energy, respectively. The investigated contact charges were positioned near the central region of the wall, and the resulting damage was concentrated primarily around the charge location. For configurations without complete brick detachment, the response was limited to local cracking and damage rather than complete wall failure. Table 10 summarizes the debris response and observed damage states for all investigated charge configurations. The SPH3 and CYH3 configurations, which retained the same explosive mass as SPH2 and CYH2, respectively, but used lower explosive density and larger charge volume, did not produce complete brick detachment. In contrast, CYV3, which had the same 4-kg explosive mass and the same density-volume combination as CYH3 but a different charge orientation, still resulted in complete wall failure. This comparison indicates that charge

orientation can also influence the structural response when the explosive mass, density, and volume are similar.

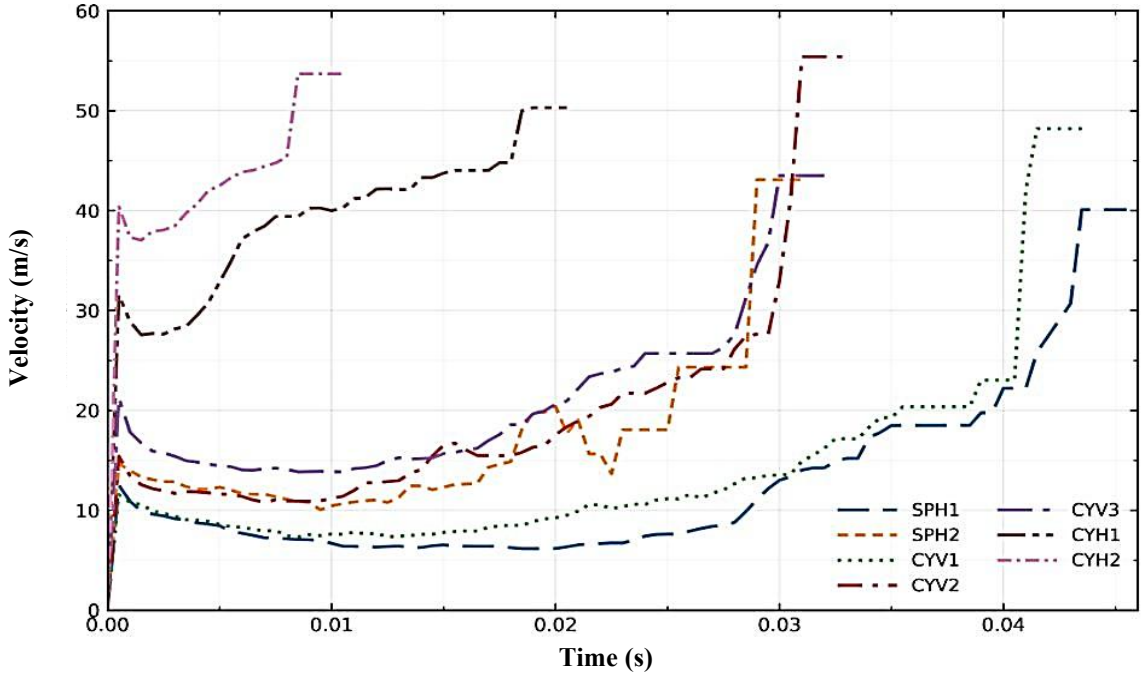


Fig. 15. Time histories of the velocity of representative detached bricks for the investigated explosive configurations.

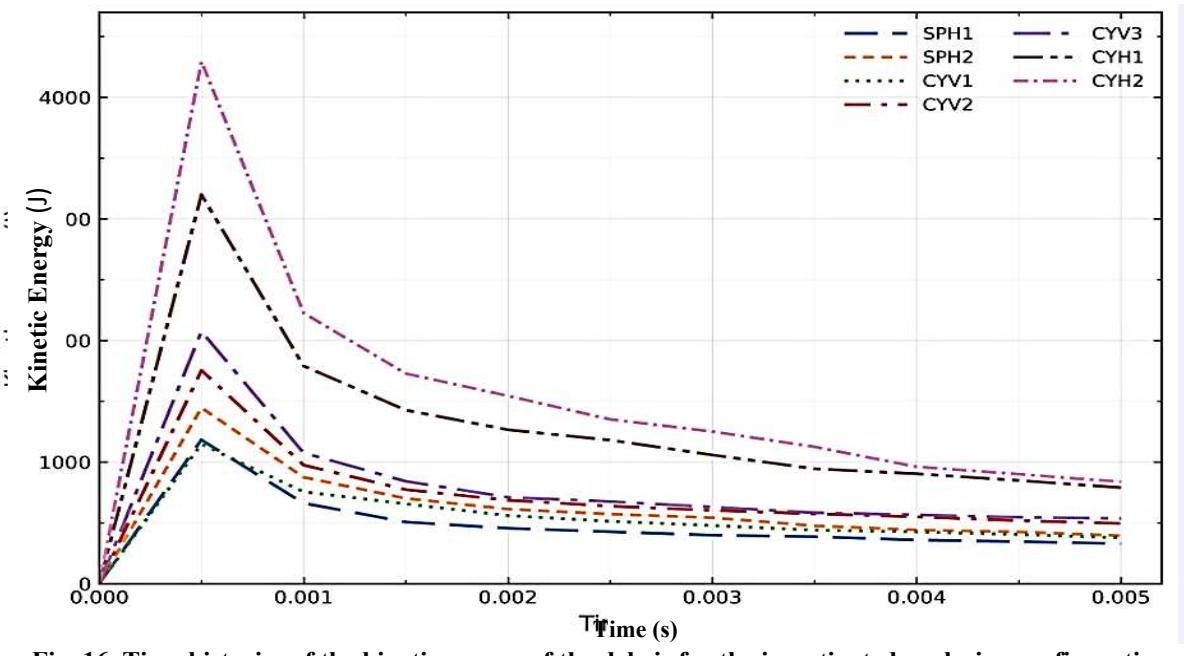


Fig. 16. Time histories of the kinetic energy of the debris for the investigated explosive configurations.

The maximum debris velocity was determined from the velocity histories of the detached bricks. The maximum debris kinetic energy was obtained from the total translational kinetic

energy of the detached bricks tracked during the simulation. The maximum values were extracted over the simulated time interval. The mass of the first detached brick was reported separately to characterize the representative detached fragment.

Table 10. Debris response and observed damage states of the investigated masonry wall configurations.

Model	Maximum debris velocity (m/s)	Maximum debris kinetic energy (J)	Mass of the first detached brick (kg)	Observed damage state
Cu 1	67.1	2040	1.31	Wall failure
SPH 1	40	1180	1.9	Wall failure
SPH 2	43.1	1450	1.11	Cracking without complete failure
SPH 3	-	-	-	Cracking without complete failure
CYV 1	48.2	1150	1.9	Wall failure
CYV 2	55.4	1750	1.75	Wall failure
CYV 3	43.5	2070	1.89	Wall failure
CYH 1	50.3	4290	0.62	Wall failure
CYH 2	53.7	3200	0.86	Cracking without complete failure
CYH 3	-	-	-	Cracking without complete failure

"–" indicates that no complete brick detachment occurred; therefore, the maximum debris velocity, maximum debris kinetic energy, and mass of the first detached brick were not reported for these configurations. Table 10 and Figs. 15–16 show that the maximum debris velocity and kinetic energy do not necessarily follow the same trend. Among the approximately 1-kg configurations, the cubic charge produced the highest maximum debris velocity (67.1 m/s), whereas the parallel cylindrical charge produced the highest maximum debris kinetic energy (4290 J). Similarly, CYV3 exhibited a lower maximum debris velocity than CYV2 (43.5 versus 55.4 m/s), while its maximum debris kinetic energy was higher (2070 versus 1750 J). These results indicate that debris velocity and kinetic energy describe different aspects of the structural response and should be considered together with the observed damage state. The comparisons among the 4-kg configurations further demonstrate that charge mass alone is insufficient to characterize the damage response. In SPH2–SPH3 and CYH2–CYH3, the charge mass remained constant while density and volume changed, resulting in markedly different damage states. The masonry response depends on the coupled effects of charge mass, density, volume, geometry, and orientation. Because several of these parameters vary simultaneously in the investigated configurations, the present results should be interpreted as configuration-dependent responses rather than as isolated effects of individual explosive parameters.

Figs. 17–19 show the damage patterns produced by the different explosive materials for the cubic charge attached to the wall. Among the investigated configurations, HMX produced the highest maximum debris velocity and the largest observed damage area. Table 11 shows that the maximum debris velocity obtained for HMX was 116.3 m/s. This response is associated

with the combined effects of explosive density, detonation velocity, explosive energy, and charge mass. Because the explosive materials have different densities, detonation velocities, JWL parameters, and corresponding charge volumes, the individual effects of explosive type and its physical properties cannot be isolated independently from the present comparisons. The quantitative comparison in Table 11 also shows that the increase in debris velocity for HMX is accompanied by an increase in the maximum debris kinetic energy. Relative to TNT, the maximum debris velocity increased from 67.1 to 116.3 m/s, corresponding to an increase of approximately 73%, while the maximum debris kinetic energy increased from 2040 to 3640 J, corresponding to an increase of approximately 78%. HNS and Tetryl produced intermediate responses, with maximum debris velocities of 77.8 and 81.9 m/s, respectively. These results indicate that the choice of explosive material can substantially modify both the velocity and energy characteristics of the debris response under the investigated contact-detonation configuration.

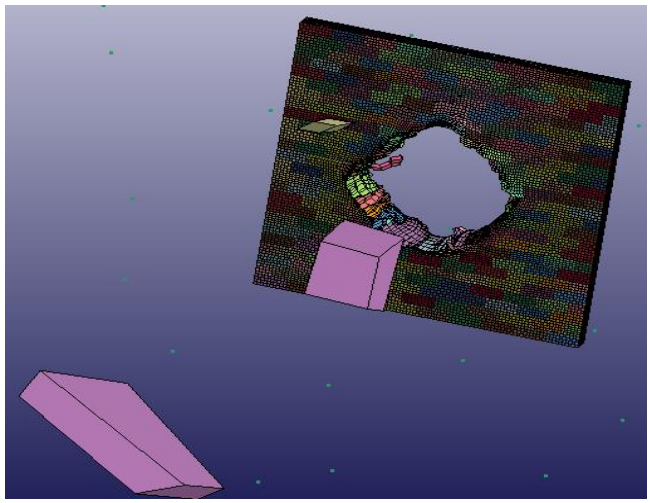


Fig. 17. Damage pattern of the brick wall subjected to contact detonation of HMX.

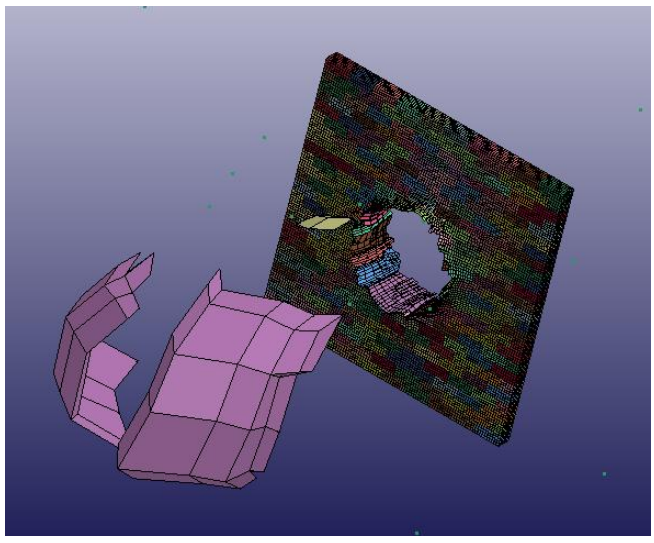


Fig. 18. Damage pattern of the brick wall subjected to contact detonation of HNS.

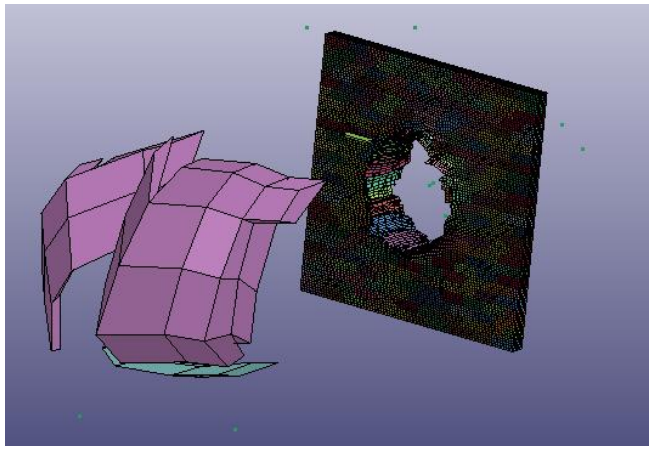


Fig. 19. Damage pattern of the brick wall subjected to contact detonation of Tetryl.

The results indicate that HMX produced the highest maximum debris velocity and kinetic energy among the investigated explosive configurations. However, the explosive materials differed in charge mass, density, detonation velocity, and JWL parameters. Therefore, the observed differences represent the combined effects of these parameters rather than the independent effect of explosive type.

Table 11. Debris response of the masonry wall for different explosive types.

Type of explosive	Maximum velocity of the thrown brick (m/s)	Maximum kinetic energy during explosion (J)	The mass of the first brick thrown (kg)
TNT	67.1	2040	1.31
HMX	116.3	3640	1.39
HNS	77.8	3020	1.54
TETRYL	81.9	3180	1.59

7. Conclusion

In this study, the effects of explosive geometry, charge mass, charge density, and explosive type on the blast-induced damage and debris response of an unreinforced brick masonry wall subjected to contact detonation were investigated using LS-DYNA. The numerical approach was assessed against the 1-kg contact-detonation configuration reported in Ref. [21]. The maximum debris velocity obtained in the present simulation was 67.1 m/s, compared with approximately 70 m/s in the reference numerical model and 80 m/s in the corresponding experiment. The difference from the reference numerical result was 4.14%, providing a partial assessment of the numerical approach for the investigated configuration. Among the investigated approximately 1-kg contact-detonation configurations, the cubic charge produced the highest maximum debris velocity, followed by the parallel cylindrical, perpendicular cylindrical, and spherical configurations. Because the charge geometries differ simultaneously in contact area, dimensions, and spatial distribution of the explosive material, the comparison represents the response of the investigated configurations rather than an isolated geometry effect. For the investigated 4-kg configurations, increasing the charge volume while reducing the explosive density produced different responses depending on the charge geometry and orientation. No complete brick detachment was observed for the SPH3 and CYH3 configurations, whereas CYV3 still exhibited wall failure. For the perpendicular cylindrical configuration, the maximum debris velocity decreased from 55.4 to 43.5 m/s, while the

maximum debris kinetic energy increased from 1750 to 2070 J. These results indicate that the effects of charge density and volume depend on the overall charge configuration. Among the investigated explosive materials, HMX produced the highest maximum debris velocity in the corresponding cubic contact-detonation configuration. However, because the explosive materials have different densities, detonation velocities, JWL parameters, and corresponding charge volumes, the present comparison does not isolate the independent contribution of any single explosive property. A limitation of the present study is that the surrounding air was not explicitly modeled. Consequently, the present results are limited to contact detonation and do not account for aerodynamic drag during subsequent debris flight. Future work should incorporate an appropriate air-domain or blast-load formulation to investigate stand-off detonations and air-mediated debris transport.

Funding
The authors did not receive support from any organization for the submitted work.

Conflict of interest
On behalf of all authors, the corresponding author states that there is no conflict of interest.

Data Availability
The datasets generated during and/or analyzed during the current study are available from the corresponding author on reasonable request.

References
[1] Bergami, A.V.: Implementation and experimental verification of models for nonlinear analysis of masonry infilled R.C. frames. PhD thesis, Università degli Studi Roma Tre, Rome (2008).

[2] Grabowski, S.: Material properties for the tests in WP 7 and 8 and the verification of the design model of WP 4. ESECMaSE Project, Technische Universität München, Munich (2005).

[3] Lourenço, P.B.: Computational strategies for masonry structures. PhD thesis, Delft University of Technology, Delft (1996).

[4] Barraza, J.A.C.: Numerical model for nonlinear analysis of masonry walls. PhD thesis, RWTH Aachen University, Aachen (2012).

[5] Giambanco, G., Di Gati, L.: A cohesive interface model for the structural mechanics of block masonry. Mech. Res. Commun. 24, 503–512 (1997). https://doi.org/10.1016/S0093-6413(97)00055-4

[6] Burnett, S., Gilbert, M., Molyneaux, T., Beattie, G., Hobbs, B.: The performance of unreinforced masonry walls subjected to low-velocity impacts: finite element analysis. Int. J. Impact Eng. 34, 1433–1450 (2007). https://doi.org/10.1016/j.ijimpeng.2006.08.004

[7] Lopez, J., Oller, S., Oñate, E., Lubliner, J.: A homogeneous constitutive model for masonry. Int. J. Numer. Methods Eng. 46, 1651–1671 (1999). https://doi.org/10.1002/%28SICI%291097-0207%2819991210%2946%3A10%3C1651%3A%3AAID-NME718%3E3.0.CO%3B2-2

[8] Anthoine, A.: Derivation of the in-plane elastic characteristics of masonry through homogenization theory. Int. J. Solids Struct. 32, 137–163 (1995). https://doi.org/10.1016/0020-7683(94)00140-R

[9] Chen, S.Y., Moon, F.L., Yi, T.: A macroelement for the nonlinear analysis of in-plane unreinforced masonry piers. Eng. Struct. 30, 2242–2252 (2008). https://doi.org/10.1016/j.engstruct.2007.12.001

[10] Bogosian, D., Gerber, B.: Analytical predictions of fragment penetration through hollow concrete masonry units. Shock Vib. 15, 61–70 (2008). https://doi.org/10.1155/2008/586876

[11] Randers-Pehrson, B., Bannister, K.A.: Airblast loading model for DYNA2D and DYNA3D. Technical Report ARL-TR-1310, U.S. Army Research Laboratory, Aberdeen Proving Ground, MD (1997).

[12] Wang, J.: Simulation of landmine explosion using LS-DYNA3D software: benchmark work of simulation of explosion in soil and air. DSTO Aeronautical and Maritime Research Laboratory, Fishermans Bend (2001).

[13] Williams, K., McClennan, S., Durocher, R., St-Jean, B., Tremblay, J.: Validation of a loading model for simulating blast mine effects on armoured vehicles. In: Proceedings of the 7th International LS-DYNA Users Conference, Dearborn, MI, USA, pp. 35–44 (2002).

[14] Kingery, C.N., Bulmash, G.: Airblast parameters from TNT spherical air burst and hemispherical surface burst. Technical Report ARBRL-TR-02555, U.S. Army Ballistic Research Laboratory, Aberdeen Proving Ground, MD (1984).

[15] Lin, Y.-W., Lawley, D., Wotherspoon, L., Ingham, J.M.: Out-of-plane testing of unreinforced masonry walls strengthened using ECC shotcrete. Structures 7, 33–42 (2016). https://doi.org/10.1016/j.istruc.2016.04.005

[16] Lin, Y.-W., Wotherspoon, L., Scott, A.N., Ingham, J.M.: In-plane strengthening of clay brick unreinforced masonry wallettes using ECC shotcrete. Eng. Struct. 66, 57–65 (2014). https://doi.org/10.1016/j.engstruct.2014.01.043

[17] Maalej, M., Lin, V.W.J., Nguyen, M.P., Quek, S.T.: Engineered cementitious composites for effective strengthening of unreinforced masonry walls. Eng. Struct. 32, 2432–2439 (2010). https://doi.org/10.1016/j.engstruct.2010.04.017

[18] Dizhur, D., Griffith, M., Ingham, J.: Out-of-plane strengthening of unreinforced masonry walls using near-surface-mounted fibre-reinforced polymer strips. Eng. Struct. 59, 330–343 (2014). https://doi.org/10.1016/j.engstruct.2013.10.026

[19] Khooshechi, M., Tanzadeh, J.: Experimental and mechanical performance of shotcrete made with nanomaterials and fiber reinforcement. Constr. Build. Mater. 165, 199–205 (2018). https://doi.org/10.1016/j.conbuildmat.2017.12.199

[20] Mardani, A., Raissi Dehkordi, M., Moghadam, A.S., Yekrangnia, M.: Example of a two-story unreinforced masonry building retrofitted by shotcrete. In: Yekrangnia, M., Arian, S. (eds.) Advanced Design Examples of Seismic Retrofit of Structures, pp. 13–118. Butterworth-Heinemann, Oxford (2019). https://doi.org/10.1016/B978-0-08-102534-5.00002-7

[21] Michaloudis, G., Gebbeken, N.: Modeling masonry walls under far-field and contact detonations. Int. J. Impact Eng. 123, 84–97 (2019). https://doi.org/10.1016/j.ijimpeng.2018.09.019

[22] Darban, H.R.: Introduction to LS-DYNA software. Malek Ashtar University of Technology, Tehran (2022).